Review of crystal and domain structures in the $PbZr_xTi_{1-x}O_3$ solid solution

David I. Woodward,[1,*] Jesper Knudsen,[2] and Ian M. Reaney[1]
[1]*Department of Engineering Materials, University of Sheffield, Sir Robert Hadfield Building, Mappin Street, Sheffield, S1 3JD, United Kingdom*
[2]*Risø National Laboratory, Materials Research Department, Building 228, Frederiksborgvej 399, DK-4000, Roskilde, Denmark*
(Received 12 May 2005; published 20 September 2005)

Several intermediate phases have recently been identified in the $PbZr_xTi_{1-x}O_3$ (PZT) phase diagram, located close to the antiferroelectric-ferroelectric and morphotropic phase boundaries. Superlattice reflections from some of these phases are clearly visible in the appropriate electron diffraction patterns and have therefore been used to provide further information concerning their symmetry. Here, the structural distortions giving rise to the new phases are discussed and their domain structures compared with those of tetragonal and rhombohedral PZT. Coherent structural arguments are presented to explain the observed phase transition sequences.

DOI: 10.1103/PhysRevB.72.104110 PACS number(s): 77.84.Dy, 68.37.Lp, 61.50.Ah, 61.14.Lj

I. INTRODUCTION

Ceramics based on $PbZr_xTi_{1-x}O_3$ (PZT) are used in sensors and actuators due to their high piezoelectric and coupling coefficients first measured by Berlincourt *et al.*[1] The phase diagram determined by Jaffe *et al.*[2] (Fig. 1) shows a largely temperature-independent phase boundary between rhombohedral and tetragonal phases at approximately equal concentrations of Zr^{4+} and Ti^{4+}. The term "Morphotropic phase boundary" (MPB) was introduced to describe this phase boundary although evidence exists for the coexistence of rhombohedral and tetragonal phases at the MPB at room temperature.[3] All compositions on the Ti-rich side of the MPB are tetragonal with *P*4*mm* symmetry, but several more phase boundaries occur on the Zr-rich side. The rhombohedral structure at high temperature has space group *R*3*m* indicating that the average cation displacements are along the $[111]_p$ direction (where p=pseudocubic). A phase transition to *R*3*c* occurs on cooling as a result of antiphase tilting of the oxygen octahedra about the $[111]_p$ axis ($a^-a^-a^-$ tilt system).[4] Close to the $PbZrO_3$ end, a ferroelectric (FE) to antiferroelectric (AFE) phase boundary is encountered which is characterised by the cations adopting an antiparallel arrangement along $[110]_p/[\bar{1}\bar{1}0]_p$ directions in the AFE phase. This arrangement is coupled to antiphase rotations of the octahedra around the $[110]_p$ axis ($a^-a^-c^0$ tilt system), giving *Pbam* symmetry.

This information represents the accepted view of the PZT phase diagram that persisted until the late 1990s, at which time new data began to emerge for the existence of low-symmetry phases which principally occur close to the AFE-FE and morphotropic phase boundaries. This paper reviews the evidence for the new phases and presents an overview of the structural changes which occur in the Zr-rich side of the phase diagram. All new data was obtained from samples that were attrition-milled to submicron particle sizes prior to and immediately following calcination. These data are consistent with those obtained in the reviewed articles and consequently the materials are considered to be macroscopically homogeneous. The data are principally based on electron diffraction since this technique most clearly elucidates the superlattice reflections associated with some of the intermediate phases. In addition, imaging with transmission electron microscopy allows the typical domain structures to be characterized.[5] For simplicity of comparison, all planes and vectors are indexed in the pseudocubic setting.

II. THE ANTIFERROELECTRIC-FERROELECTRIC PHASE BOUNDARY

Materials made in a narrow range of compositions close to the AFE-FE phase boundary ($x \approx 0.94$) have yielded electron diffraction patterns that are inconsistent with both *Pbam* and *R*3*c* models. Two distinct models are proposed to account for these observations, but first, the evidence for the existence of these phases is presented.

At $x=1$ (undoped $PbZrO_3$), some $\langle 100\rangle_p$ and $\langle 111\rangle_p$ zone axis electron diffraction patterns (ZADPs) contain $1/4\{hk0\}_p$ superlattice reflections [Fig. 2(a)], due to the antipolar cation displacements leading to quadrupling of the unit cell along one of the $\langle 110\rangle_p$ directions (Sawaguchi *et al.*[6]). The AFE cell has *Pbam* symmetry and has dimensions

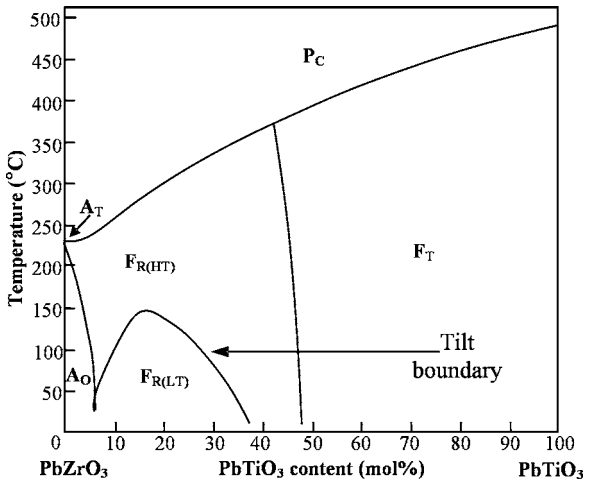

FIG. 1. A reproduction of the original PZT phase diagram as determined by Jaffe *et al.* (Ref. 2).

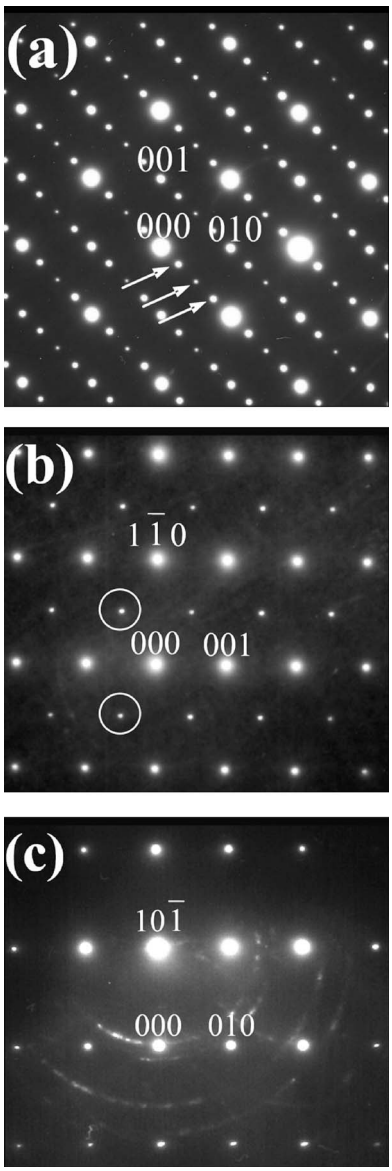

FIG. 2. ZADPs from $PbZrO_3$ (a) $\langle 100\rangle_p$ zone axis with $1/4\{hk0\}_p$ superlattice reflections (arrowed) and two variants of the $\langle 110\rangle_p$ ZADPs (b) with $1/2\{hkl\}_p$ reflections (ringed) and (c) without.

$\sim\sqrt{2}a_o\times 2\sqrt{2}a_o\times 2a_o$, where a_o is the lattice parameter of the pseudocubic perovskite subcell.[7] Reflections due to the antipolar cation displacements are forbidden in $\langle 110\rangle_p$ ZADPs according to the Weiss zone law, since the intensities of type $1/4\{hk0\}_p$ are subject to the constraint $h\neq k$. Moreover, in $\langle 110\rangle_p$ oriented grains, the $1/2\{hkl\}_p$ reflections arising from antiphase rotations of the oxygen octahedra are absent from some domains [Figs. 2(b) and 2(c)] indicating domain variance consistent with the $a^-a^-c^0$ tilt system of $PbZrO_3$. Simulations of the *Pbam* cell indicate that only 10/12 of the $\langle 110\rangle_p$ ZADPs exhibit reflections associated with antiphase rotations of the octahedra.

At $x=0.95$, $\langle 110\rangle_p$ ZADPs were obtained that contained $1/2\{hk0\}_p$ but not $1/4\{hk0\}_p$ reflections [Fig. 3(a)], inconsistent with the structures of $PbZrO_3$ and both the low- and high-temperature rhombohedral phases. The $1/2\{hk0\}_p$ reflections became progressively weaker as x decreased [Fig. 3(b)] becoming absent at room temperature by $x=0.7$ [Fig. 3(c)]. The $1/2\{hkl\}_p$ reflections were not present in any $\langle 110\rangle$ ZADPs at $x=0.95$ [Fig. 3(a)] but were observed weakly in $\langle 110\rangle_p$ ZADPs at $x=0.9$ [Fig. 3(b)],[8] increasing in intensity as x decreased [Fig. 3(c)]. It should be noted that in transmission electron microscopy (TEM), under conventional parallel beam illumination conditions, heating due to the electron beam is estimated to increase the sample temperature by 50–80 °C.[9] The absence of $1/2\{hkl\}_p$ reflections at $x=0.95$ but their presence at $x=0.9$ is therefore consistent with the original phase diagram (Fig. 1). However, according to the phase diagram, compositions in the range $0.6<x<0.95$ have $R3c$ symmetry at room temperature for which $1/2\{hk0\}_p$ reflections are forbidden. The electron diffraction data therefore indicate that for $x=0.95$ and 0.9 the local symmetry is inconsistent with the original phase diagram. It is evident therefore that some form of structural distortion results in $1/2\{hk0)_p$ reflections in both compositions, while antiphase tilting, though present at $x=1$ and 0.9, is absent at $x=0.95$. Many authors have recognized the presence of at least one intermediate phase near the AFE-FE phase boundary, but there is little agreement concerning the symmetries present or the mechanism that generates the $1/2\{hk0\}_p$ reflections.

The perovskite tolerance factor, t, is defined as

$$t=\frac{(R_A+R_O)}{\sqrt{2}(R_B+R_O)}, \tag{1}$$

where R_A, R_B and R_O are the average ionic radii for the A- and B-site cations and oxygen anions, respectively. In the PZT series, as x increases, t decreases. Low tolerance factors ($t<0.985$) favor tilted perovskite structures and the phase assemblage of the PZT phase diagram obeys this general principle with the onset of tilting occurring at room temperature at around $x=0.6$. Moreover, as x increases, the onset temperature for tilting, denoted by the $R3m-R3c$ phase boundary, initially increases. However, the subsequent fall in this transition temperature across the range $0.85<x<0.95$ and the absence of antiphase tilt reflections at $x=0.95$ followed by their reappearance at $x>0.95$ are anomalous and do not conform to the general behavior of perovskites, where the convention is for the tilt transition temperature to monotonically increase as t decreases (Reaney *et al.*[10]).

Viehland[11] and Xu *et al.*[12] suggested that the $1/2\{hk0\}_p$ reflections arise from in-phase rotations of octahedra. However, according to Glazer,[4] $1/2\{hk0\}_p$ reflections generated by in-phase tilting of oxygen octahedra are subject to the condition $h\neq k$. The reflections must therefore be absent from all $\langle 110\rangle_p$ ZADPs. In addition, according to Reaney *et al.*,[10] in-phase tilting is particularly unlikely to occur in perovskites with a relatively high tolerance factor of $t>0.98$, as is the case here. Octahedral tilting therefore seems an unlikely source of the $1/2\{hk0\}_p$ superlattice reflections. Two other mechanisms may generate superlattice reflections in stoichiometric perovskites: cation ordering and antiparallel cation displacements. Only small amounts of Ti^{4+} are substituted in place of Zr^{4+} and the two cations have equal valence

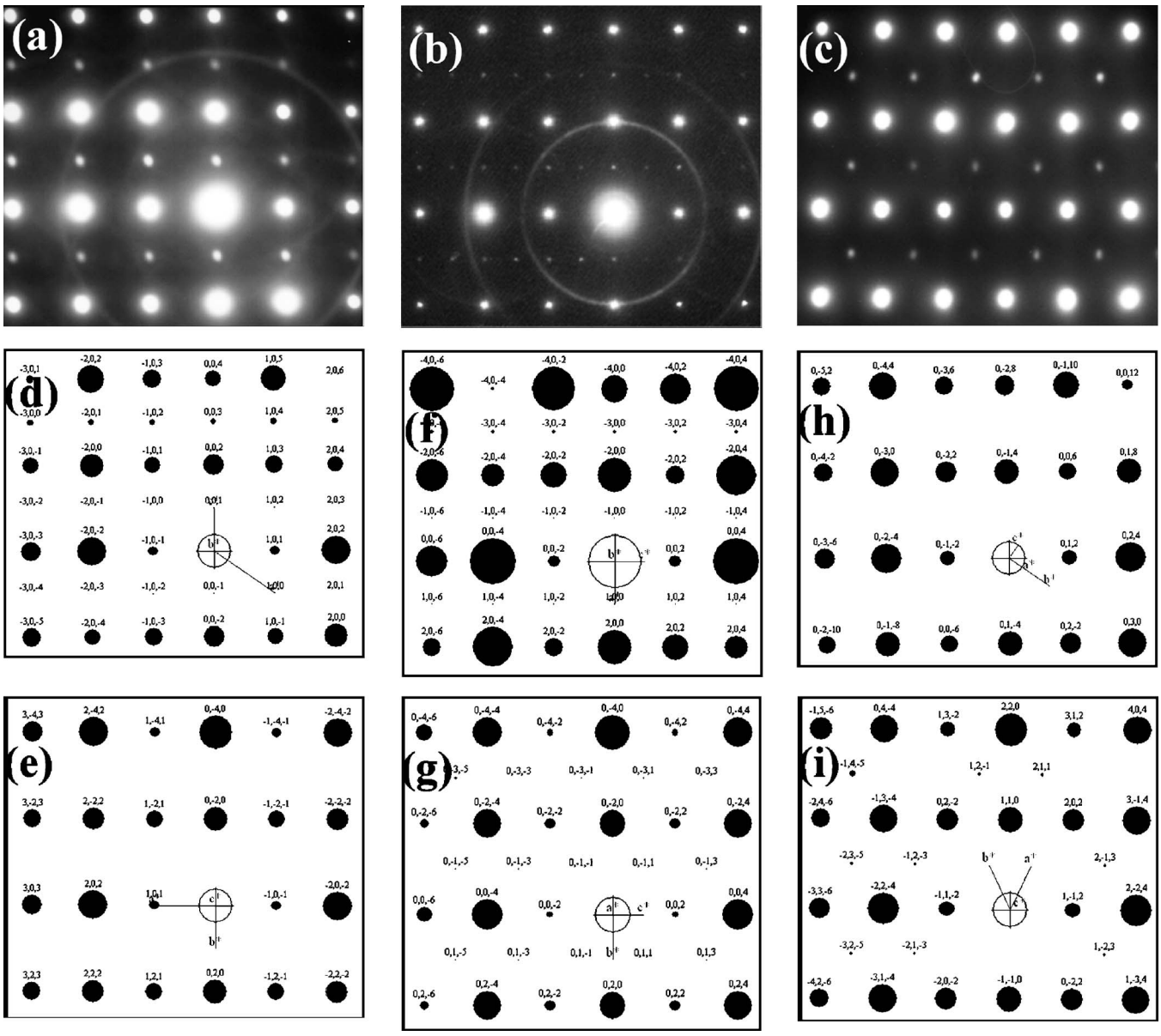

FIG. 3. Multiple-domain $\langle 110\rangle_p$ ZADPs from samples with compositions (a) $x=0.95$, (b) $x=0.9$, and (c) $x=0.7$. The simulations have been obtained using (d),(e) the *Pm* cell, (f),(g) the *Pc* cell attributed to Knudsen *et al.* (Ref. 14), and (h),(i) the *R*3*c* cell refined by Corker *et al.* (Ref. 16). These illustrate all variants of the $\langle 110\rangle_p$ ZADPs for each model.

states. Hence, there is no driving force for ordering on the *B* site and this mechanism may be ruled out. By a process of elimination, $1/2\{hk0\}_p$ reflections must arise from antiparallel displacements of the cations, as suggested by Reaney *et al.*[13] for the related $(Pb_{1-x}Ba_x)(Zr_{1-x}Ti_x)O_3$ solid solution on the basis of similar diffraction data.

A model was recently proposed by Knudsen *et al.*[14] for an intermediate structure between FE and AFE structures in La-doped PZT. This monoclinic cell with space group *Pc* was based on electron diffraction data and allows a continuous transition in both tilt axis and polarization vector as a function of composition from rhombohedral FE to orthorhombic AFE structures. These observations have been supported by several research groups (e.g., Reaney *et al.*;[13] Ricote *et al.*[15]) who investigated the AFE-FE phase boundary region of PZT and related systems. However, it is only the work of Knudsen *et al.*[14] which proposes a unique phase for this region of the phase diagram.

This unit cell, illustrated in Fig. 4, accounts for all diffraction patterns observed in PZT at $x=0.9$. The authors proposed that, although close to the AFE-FE phase boundary the Pb^{2+} ions have an average displacement along $\langle 111\rangle_p$, locally, they displace slightly away from this direction with a component along a $\langle 110\rangle_p$ direction in one layer but an antiparallel component in the layer immediately above. This doubles the unit cell normal to some $\{hk0\}_p$ planes. The tilt axis is coupled to the local polarization vectors, stabilizing an $a^-b^-b^-$ tilt system which is intermediate between the $a^0b^-b^-$ and $a^-a^-a^-$ tilt systems of the *Pbam* (AFE) and *R*3*c* (FE) phases, respectively. The $\langle 110\rangle_p$ and $\langle 111\rangle_p$ components

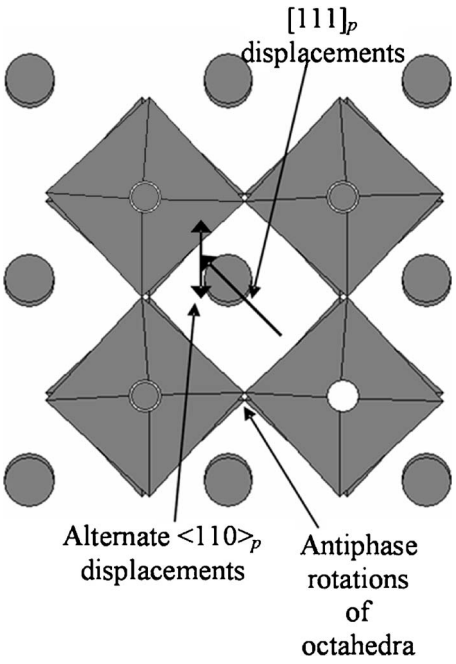

FIG. 4. $[001]_p$ projection of the *Pc* cell proposed by Knudsen *et al.* (Ref. 14) to exist at the AFE-FE phase boundary.

of the Pb^{2+} displacements are also associated with the *Pbam* and *R*3*c* cells, respectively.

At room temperature in a narrow compositional range around $x=0.95$, no $1/2\{hkl\}_p$ tilt reflections are observed by electron diffraction in any $\langle 110\rangle_p$ ZADPs, but the $1/2\{hk0\}_p$ reflections associated with the *Pc* model are present. We therefore propose a new unit cell with space group *Pm* to account for these observations. This space group does not allow tilting to occur but does allow the Pb^{2+} ions to displace with the same vectors as in the *Pc* model and is thus consistent with the diffraction data. Simulations of the appropriate $\langle 110\rangle_p$ ZADPs are shown in Fig. 3 for the proposed *Pm* symmetry at $x=0.95$ [Figs. 3(d) and 3(e)], the *Pc* cell of Knudsen *et al.*[14] [Figs. 3(f) and 3(g)] and the *R*3*c* cell refined by Corker *et al.*[16] [Figs. 3(h) and 3(i)].

The stabilization of an intermediate phase implies the presence of Zr-rich clusters of ions near the AFE-FE phase boundary. Phase transformations of Zr-rich regions are frustrated by the surrounding matrix and consequently adopt a structure that is intermediate between AFE and FE. The volume fraction of the intermediate phase logically increases as the Zr concentration increases (x increases) until they are of sufficient size and number to stabilize the AFE *Pbam* cell. Such cluster models across phase boundaries are becoming increasingly accepted to explain the presence of low-symmetry phases at phase boundaries (Glazer[17]).

In PZT, the octahedral rotations are directly coupled to the displacement of the Pb^{2+} ions. If these displacements become frustrated, it follows that the octahedral rotations also become frustrated, leading to shorter coherence lengths and a resultant decrease in the onset temperature of the tilt transition. This model explains not only the diffraction data presented in Fig. 3, but also the anomalous decrease in the tilt transition temperature in the range $0.85<x<0.95$ and the absence of tilting at ambient TEM conditions encountered at $x=0.95$.

III. THE MORPHOTROPIC PHASE BOUNDARY

The PZT phase diagram remained largely unchanged until Noheda *et al.*[18] published neutron diffraction data demonstrating the existence of a low-temperature monoclinic phase separating rhombohedral and tetragonal structures at $x=0.52$. This structure is derived from the tetragonal cell by displacement of the Pb^{2+} ions along the $[001]_p$ axis with an added component along $[110]_p$ and has space group *Cm*. The presence of this monoclinic structure allows a continuous transition between the rhombohedral and tetragonal ferroelectric displacements.

Prior to the published work of Noheda *et al.*,[18] a neutron diffraction study by Corker *et al.*[16] focused attention on the anisotropic temperature factors obtained from the refinement process for compositions in the PZT series with $0.08\leqslant x\leqslant 0.38$. They found strongly anisotropic thermal parameters indicating that the Pb^{2+} ions were in fact displaced primarily along the $[111]_p$ direction but with an additional shift along one of the three component $\langle 100\rangle_p$ directions. They suggested that locally, Pb^{2+} displacements are not purely along $[111]_p$ but include an off-axis displacement that averages to zero. Recently, Glazer[17] has proposed that as the MPB is approached, unit cells containing same-axis displacements begin to cluster. As the clusters exceed a certain size, the perceived (average) structure is no longer rhombohedral and is in fact the monoclinic unit cell. Further movement of the polarization vector ultimately results in the tetragonal structure.

In a recent publication, Ragini *et al.*[19] presented $\langle 110\rangle_p$ ZADPs obtained from a PZT sample at $x=0.515$. These diffraction patterns exhibited $1/2\{hkl\}_p$ superstructure reflections at <200 K. The reflections had not been observed by Noheda *et al.*[18] with neutron or x-ray diffraction techniques and while they are inconsistent with the *Cm* model, they are consistent with the onset of antiphase tilting. Similar diffraction patterns from a sample at $x=0.5$ are shown in Fig. 5 and illustrate as a function of temperature the evolution of the $1/2\{hkl\}_p$ reflections.

Ranjan *et al.*[20] proposed a model with space group *Pc* based on neutron diffraction, combining the displacements of the *Cm* model with an $a^0a^0c^-$ tilt system. Hatch *et al.*[21] showed that the correct space group for this was in fact *Cc*. However, these reports overlooked the fact that the tilt system is not constrained by space group *Cc* to be $a^0a^0c^-$ and is in fact permitted to be $a^-b^-b^-$, thus allowing the ionic displacements and the tilt axis to have the same vector. A projection of this structure is shown in Fig 6.

Noheda *et al.*[22] also published electron diffraction patterns exhibiting $1/2\{hkl\}_p$ reflections obtained at $x=0.52$ at 87 K. They showed that the superstructure reflections varied in intensity between regions and included dark field images formed from the superstructure reflections. The dark field images showed a domain structure with a particularly fine scale of the order of a few nm. They interpreted these results as showing the coexistence of both *Cm* and *Cc* phase at low

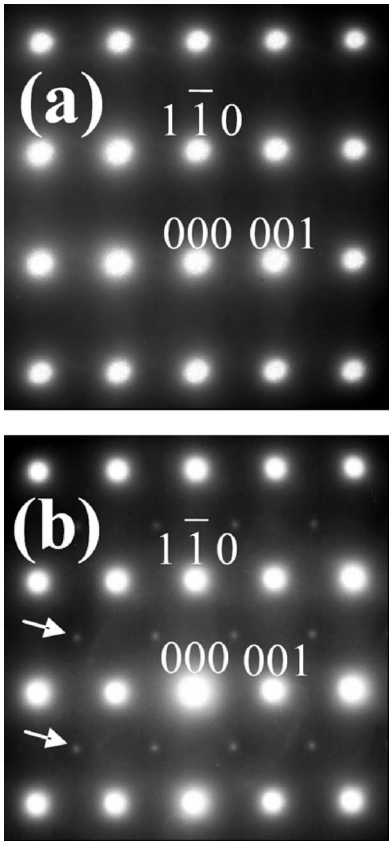

FIG. 5. $\langle 110\rangle_p$ ZADPs from an $x=0.5$ sample obtained at (a) room temperature and (b) 20 K illustrating the temperature-dependent evolution of the $1/2\{hkl\}_p$ reflections (arrowed) associated with antiphase tilting.

temperatures. However, leaving aside the possibility of variations in sample thickness leading to observed differences in the intensity of the superstructure reflections, these observations are in fact entirely consistent with the *Cc* phase. The tilt system $a^-b^-b^-$ allows variations in intensity of the superstructure reflections. Of the 12 possible $\langle 110\rangle_p$ zone axes, 2 will not exhibit $1/2\{hkl\}_p$ reflections, 6 will exhibit relatively strong $1/2\{hkl\}_p$ reflections and the remaining 4 will show $1/2\{hkl\}_p$ reflections that decrease in intensity as the magnitude of a approaches that of b (Woodward and Reaney[23]). The splitting of higher-order reflections in the electron diffraction patterns, considered by Noheda *et al.*[22] as further evidence of a two-phase mixture is also consistent with the *Cc* model. We conclude therefore that the *Cm* model does not persist below 200 K and does not coexist with the *Cc* cell.

On the basis of our own work and the above data, in which weak $1/2\{hkl\}_p$ reflections have been observed at $\sim$ 20 K for $x=0.50$ and $x=0.52$, it is proposed that the tilted region of the PZT phase diagram extends to the MPB on cooling to 20 K, crossing the rhombohedral-monoclinic phase boundary. This creates a new phase field where the resulting structure combines the cation displacements of the *Cm* cell of Noheda *et al.*[18] with tilting, resulting in overall *Cc* symmetry.

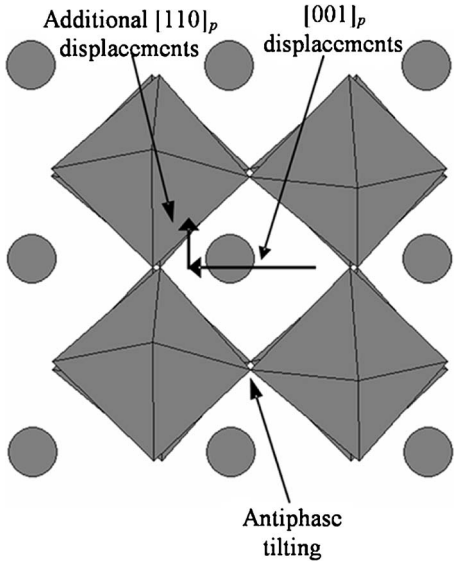

FIG. 6. $[010]_p$ projection of the low-temperature MPB monoclinic structure (*Cc*), illustrating antiphase tilting and the components of the cation displacements.

IV. FERROELECTRIC DOMAIN STRUCTURE

As suggested by Knudsen *et al.*,[14] at a phase boundary where it is anticipated that clusters of ions of different size or charge may form, there should be some physical evidence of their presence.[24] To date, there have been few reliable chemical analyses performed on PZT since it readily damages during irradiation under a focused beam and energy dispersive spectra are thereby difficult to quantify. However, the impingement of clusters gives rise to local frustration of Pb^{2+} displacements which may become manifest in the apparent domain structure.

Figures 7(a)–7(d) are bright field TEM images of PZT, $x=0.4$, 0.5, 0.6, and 0.95, which illustrate the domain structure observed in some grains at room temperature for tetragonal, MPB, rhombohedral and intermediate AFE-FE phases, respectively. The classic view of domain theory suggests that rhombohedral PZT should have polarisation vectors which intersect at domain walls at 71° and 109°, giving walls which may lie on $\{110\}_p$ and $\{100\}_p$ planes.[25,26] Similarly, the polarization vectors in tetragonal PZT should intersect at a domain wall at 90° and give domain walls which habit $\{110\}_p$ planes. Figure 7(a) (tetragonal PZT, $x=0.4$) shows lamellar domains which habit the $\{110\}_p$ planes. Similarly, Fig. 7(c) reveals a well-organized domain structure whose walls lie on low-order crystallographic planes. By contrast, Figs. 7(b) and 7(d) reveal domain structures which are coherent only over much shorter distances (20–50 nm) and whose walls do not often habit low-order crystallographic planes. The complex domain structures exhibited at $x=0.5$ and 0.95 are believed to be a physical manifestation of the frustration between and Zr- and Ti-rich clusters.

Care must be taken with this type of analysis since domain structures may be readily rearranged *in situ* during irradiation by the electron beam and consequently it is the view of the authors that too much emphasis can be placed on

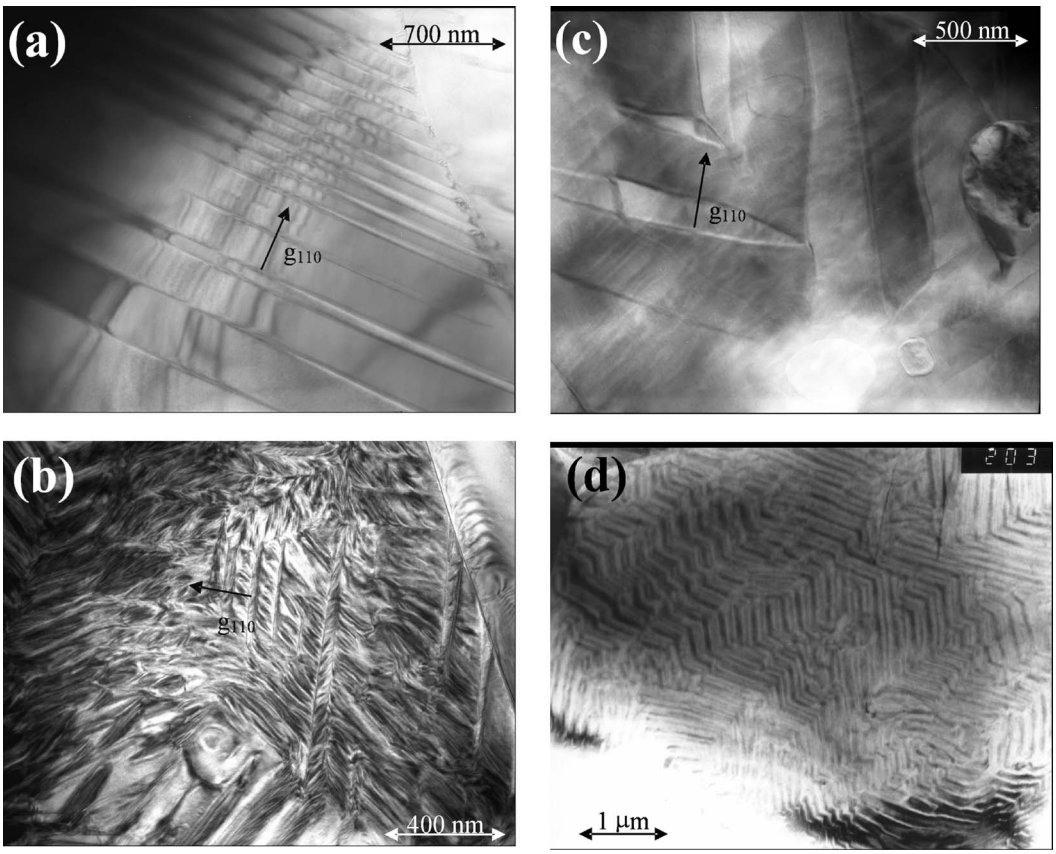

FIG. 7. Bright field images of typical domain structure encountered across the PZT series. (a) $x=0.4$; tetragonal domains imaged parallel to $\langle 001\rangle_p$, (b) $x=0.5$; domains observed close to MPB, imaged parallel to $\langle 001\rangle_p$, (c) $x=0.6$; rhombohedral domains imaged parallel to $\langle 001\rangle_p$, (d) $x=0.95$; domains observed near AFE-FE boundary, beam parallel to $\langle 110\rangle_p$.

the size and orientation of habit planes of the domain walls at phase boundaries since the elastic and electric boundary conditions in a thin foil bear no resemblance to those in bulk.[27] Despite this reservation, the observation of frustrated domain structures close to phase boundaries is reproducible in the PZT system.[28] Interestingly, there were no significant changes in the domain structures on cooling $x=0.52$ samples despite the onset of transitions from $R3m$ to Cm and Cc symmetries.

V. DISCUSSION AND CONCLUSIONS

According to the work presented here and with reference to previous studies,[2,14,21,29] as x increases away from the MPB, the following tilt sequence and corresponding symmetries may be inferred at room temperature, and 20 K.

Room temperature (ambient microscope):

$$a^0a^0a^0 \Rightarrow a^-a^-a^- \Rightarrow a^-b^-b^- \Rightarrow a^0a^0a^0 \Rightarrow a^0b^-b^-$$

$$R3m \Rightarrow R3c \Rightarrow Pc \Rightarrow Pm \Rightarrow Pbam$$

$$x \approx 0.5 \Rightarrow 0.6 < x < 0.85 \Rightarrow 0.85 < x < 0.95 \Rightarrow x = 0.95 \Rightarrow x > 0.95.$$

At 20 K:

$$a^-b^-b^- \Rightarrow a^-a^-a^- \Rightarrow a^-b^-b^- \Rightarrow a^0b^-b^-$$

$$Cc \Rightarrow R3c \Rightarrow Pc \Rightarrow Pbam$$

$$x \approx 0.5 \Rightarrow 0.6 < x < 0.85^* \Rightarrow 0.85 < x < 0.95^* \Rightarrow x > 0.95^*.$$

The asterisk indicates that further low temperature data is required to establish the precise values of x for the extent of the Pc phase field.

The details and observations reviewed here have been used to propose modifications to the PZT phase diagram (Fig. 8).

(i) The phase boundary that separates tilted and untilted rhombohedral structures has been extended to cross the phase boundary between rhombohedral and monoclinic structures. This results in a small phase field with Cc symmetry, a result of combining the ionic displacements of the Cm cell with the $a^-b^-b^-$ tilt system. Cc is a subgroup of both $R3c$ and Cm and its existence is therefore entirely consistent with simple group theory.

(ii) A narrow phase field is proposed, separating AFE and rhombohedral FE structures. Within this phase field, Pb^{2+} cations are displaced along a $\langle 111\rangle_p$ direction with additional, antiparallel shifts along a $\langle 110\rangle_p$ direction. In the untilted structure, this has Pm symmetry. Introduction of the $a^-b^-b^-$ tilt system close to room temperature results in Pc

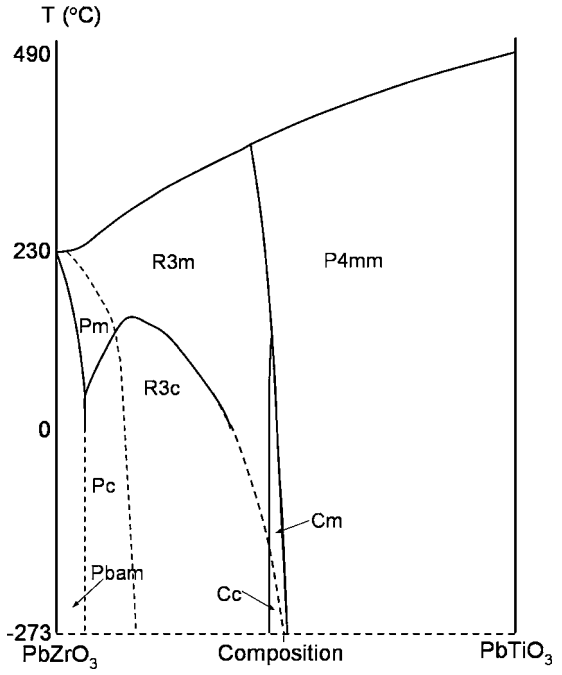

FIG. 8. The PZT phase diagram, revised to illustrate the positions of the intermediate structures. Dashed lines indicate the proposed changes that are consistent with the proposed monoclinic unit cells.

symmetry. In group theory, both symmetries are fully consistent with the proposal that these are intermediate phases; *Pm* is a subgroup of *R*3*m* and *Pbam*, while *Pc* is a subgroup of *Pm*, *Pbam* and *R*3*c*. The dashed lines in Fig. 8 are not intended to represent the exact composition or temperature locations of the phase boundaries, but are intended to illustrate how these phases are related to the primary PZT phases. For more quantitative data, high-resolution neutron and x-ray diffraction is required.

A general interpretation of displacement and tilting theory can be made from the phase diagram in Fig. 8. For any composition in the PZT series, as the material is cooled through the transition from paraelectric to ferroelectric structures, the precise *B*-site composition determines the preferred polarisation vector and coupled tilting commences at a lower temperature when the effective tolerance factor is low enough. However, in the case of intermediate structures, where the polarisation vector is not in a low-order crystallographic direction, tilting sets in at a much lower temperature than for similar compositions where the polarisation vector is along a high-order crystallographic direction such as $\langle 001 \rangle_p$ or $\langle 111 \rangle_p$. This may be an effect of the frustration that is manifest in these structures. At composition $x=0.95$, the effect is to reduce the tilt onset temperature to a value low enough to preclude tilting under ambient TEM conditions.

The domain structures observed for well-defined polarization directions, e.g. $[001]_p$ and $[111]_p$ in the tetragonal and rhombohedral phases, respectively, conform to a classical interpretation that domain walls habit low-order crystallographic planes dictated by the macroscopic symmetry. By contrast, intermediate phases give rise to frustrated domain structures in which the habit planes of the domain walls do not directly relate to the apparent macroscopic symmetry. It is postulated that these domain structures are strongly influenced by the presence of local ion clustering, which is evidently affected by ceramic processing and in particular the homogeneity of the zirconium or titanium ion distribution.

*Corresponding author. Email address:
d.woodward@sheffield.ac.uk

[1] D. A. Berlincourt, C. Cmolik, and H. Jaffe, Proc. IRE **48**, 220 (1960).
[2] B. Jaffe, W. R. Cook, and H. Jaffe, *Piezoelectric Ceramics* (Academic Press, London, 1971).
[3] M. L. A. Dass, U. Dahmen, G. Thomas, T. Yamamoto, and K Okazaki, IEEE Trans. Ultrason. Ferroelectr. Freq. Control **33**, 801 (1986).
[4] A. M. Glazer, Acta Crystallogr., Sect. A: Cryst. Phys., Diffr., Theor. Gen. Crystallogr. **31**, 756 (1975).
[5] C. A. Randall, M. G. Matsko, W. Cao, and A. S. Bhalla, Solid State Commun. **85**, 193 (1993).
[6] E. Sawaguchi, H. Maniwa, and S. Hoshino, Phys. Rev. **83**, 1078 (1951).
[7] D. L. Corker, A. M. Glazer, J. Dec, K. Roleder, and R. W. Whatmore, Acta Crystallogr., Sect. B: Struct. Sci. **53**, 135 (1997).
[8] H. Huang, L. M. Zhou, J. Guo, H. H. Hng, J. T. Oh, and P. Hing, Appl. Phys. Lett. **83**, 3692 (2003).
[9] B. G. Demczyk, R. S. Rai, and G. Thomas, J. Am. Ceram. Soc. **73**, 615 (1990).
[10] I. M. Reaney, E. L. Colla, and N. Setter, Jpn. J. Appl. Phys., Part 1 **33**, 3984 (1994).
[11] D. Viehland, Phys. Rev. B **52**, 778 (1995).
[12] Z. Xu, X. Dai, J.-F. Li, and D. Viehland, Appl. Phys. Lett. **66**, 2963 (1995).
[13] I. M. Reaney, A. Glazounov, F. Chu, A. Bell, and N. Setter, Br. Ceram. Trans. **96**, 217 (1997).
[14] J. Knudsen, D. I. Woodward, and I. M. Reaney, J. Mater. Res. **18**, 262 (2003).
[15] J. Ricote, D. L. Corker, R. W. Whatmore, S. A. Impey, A. M. Glazer, J. Dec, and K. Roleder, J. Phys.: Condens. Matter **10**, 1767 (1998).
[16] D. L. Corker, A. M. Glazer, R. W. Whatmore, A. Stallard, and F. Fauth, J. Phys.: Condens. Matter **10**, 6251 (1998).
[17] A. M. Glazer, P. A. Thomas, K. Z. Baba-Kishi, G. K. H. Pang, and C. W. Tai, Phys. Rev. B **70**, 184123 (2004).
[18] B. Noheda, D. E. Cox, G. Shirane, J. A. Gonzalo, L. E. Cross, and S.-E. Park, Appl. Phys. Lett. **74**, 2059 (1999).
[19] Ragini, S. K. Mishra, D. Pandey, H. Lemmens, and G. Van Tendeloo, Phys. Rev. B **64**, 054101 (2001).
[20] R. Ranjan, Ragini, S. K. Mishra, D. Pandey, and B. J. Kennedy, Phys. Rev. B **65**, 060102(R) (2002).
[21] D. M. Hatch, H. T. Stokes, R. Ranjan, Ragini, S. K. Mishra, D. Pandey, and B. J. Kennedy, Phys. Rev. B **65**, 212101 (2002).
[22] B. Noheda, L. Wu, and Y. Zhu, Phys. Rev. B **66**, 060103(R)

(2002).
[23] D. I. Woodward and I. M. Reaney, Acta Crystallogr., Sect. B: Struct. Sci. **61**, 387 (2005).
[24] C. A. Randall, D. J. Barber, and R. W. Whatmore, J. Microsc. **145**, 275 (1987).
[25] C. A. Randall, D. J. Barber, and R. W. Whatmore, J. Mater. Sci. **22**, 925 (1987).
[26] J. Ricote, R. W. Whatmore, and D. J. Barber, J. Phys.: Condens. Matter **12**, 323 (2000).
[27] B. Tuttle, T. Headley, C. Drewien, J. Michael, J. Voigt, and T. Garino, Ferroelectrics **221**, 209 (1999).
[28] P. G. Lucata, J. Am. Ceram. Soc. **72**, 933 (1989).
[29] B. Noheda, J. A. Gonzalo, L. E. Cross, R. Guo, S.-E. Park, D. E. Cox, and G. Shirane, Phys. Rev. B **61**, 8687 (2000).